Solutions to the Atmospheric Neutrino Problem

M. C. Gonzalez-Garcia * [a]

[a]Instituto de Física Corpuscular – C.S.I.C.
Departamento de Física Teòrica, Universitat of València
46100 Burjassot, València, Spain

In this talk I review the present status of the atmospheric neutrino anomaly and discuss some solutions that have been presented in the literature to solve this problem. In particular I review the "standard" solution in terms of neutrino oscillations as well as alternative scenarios such as the possibility of flavour changing neutrino interactions with the Earth and neutrino decay.

1. Introduction

Neutrinos produced as decay products in hadronic showers from cosmic ray collisions with nuclei in the upper atmosphere have been observed by several detectors [1–7]. Although the absolute fluxes of atmospheric neutrinos are largely uncertain, the expected ratio (μ/e) of the muon neutrino flux $(\nu_\mu + \bar{\nu}_\mu)$ over the electron neutrino flux $(\nu_e + \bar{\nu}_e)$ is robust, since it largely cancels out the uncertainties associated with the absolute flux. In fact, this ratio has been calculated [8] with an uncertainty of less than 5% over energies varying from 0.1 GeV to 100 GeV. On this resides our confidence in the long-standing atmospheric neutrino anomaly.

Super-Kamiokande high statistics observations [1] indicate that the deficit in the total ratio $R(\mu/e)$ is due to the number of neutrinos arriving in the detector at large zenith angles. The e-like events do not present any compelling evidence of a zenith-angle dependent suppression while the μ-like event rates are substantially suppressed at large zenith angles. The $\nu_\mu \to \nu_\tau$ as well as the $\nu_\mu \to \nu_s$ [9,10] oscillation hypothesis provides a very good explanation for this smaller-than-expected ratio, which is also simple and well-motivated theoretically. This led the Super-Kamiokande Collaboration to conclude that their data provide good evidence for neutrino oscillations and neutrino masses [11]. However, alternative explanations to the atmospheric neutrino data have been proposed in the literature including the possibility of flavour changing (FC) neutrino interactions in matter [12] and neutrino decay [13], the violation of relativity principles [14,15] or the violation of CPT symmetry [16].

In this talk I will review the "standard" solution in terms of neutrino oscillations as well as alternative scenarios such as the possibility of flavour changing neutrino interactions with the Earth and neutrino decay.

2. Atmospheric Neutrino Induced Events at Underground Experiments

Atmospheric neutrinos can be detected in underground detectors by direct observation of their charged current interaction inside the detector. These are the so called contained events. Contained events can be further classified into fully contained events when the produced charged lepton (either electron or muon) in the neutrino interaction does not escape the detector, and partially contained muons when the produced muon exits the detector. Super-Kamiokande has divided their contained data sample into sub-GeV events with visible energy below 1.2 GeV and multi-GeV above such cutoff. On average, sub-GeV events arise from neutrinos of several hundreds of MeV while multi-GeV events are origi-

*Talk given at the Xth Baksan School "Particles and Cosmology", 19-25 April 1999, Baksan Valley, Kabardino-Balkaria, Russia, and at the 5th International Workshop "Valencia 99: Particles in Astrophysics and Cosmology", Valencia May 3-8, 1999.

nated by neutrinos with energies of the order of several GeV. Higher energy muon neutrinos and antineutrinos can also be detected indirectly by observing the muons produced in their charged current interactions in the vicinity of the detector. These are the so called upgoing muons. Should the muon stop inside the detector, it will be classified as a "stopping" muon, (which arises from neutrinos of energies around ten GeV) while if the muon track crosses the full detector the event is classified as a "through-going" muon which is originated by neutrinos with energies of the order of hundred GeV..

Given certain neutrino conversion mechanism, the expected number of μ-like and e-like contained events, N_α, $\alpha = \mu, e$ can be computed as:

$$N_\mu = N_{\mu\mu} + N_{e\mu} \ , \qquad N_e = N_{ee} + N_{\mu e} \ , \qquad (1)$$

where

$$N_{\alpha\beta} = n_t T \int \frac{d^2\Phi_\alpha}{dE_\nu d(\cos\theta_\nu)} \kappa_\alpha(h, \cos\theta_\nu, E_\nu) \\ P_{\alpha\beta} \frac{d\sigma}{dE_\beta} \varepsilon(E_\beta) dE_\nu dE_\beta d(\cos\theta_\nu) dh \quad (2)$$

and $P_{\alpha\beta}$ is the conversion probability of $\nu_\alpha \to \nu_\beta$ for given values of $E_\nu, \cos\theta_\nu$ and h, i.e., $P_{\alpha\beta} \equiv P(\nu_\alpha \to \nu_\beta; E_\nu, \cos\theta_\nu, h)$. In the Standard Model (SM), the only non-zero elements are the diagonal ones, i.e. $P_{\alpha\alpha} = 1$ for all α. Here n_t is the number of targets, T is the experiment's running time, E_ν is the neutrino energy and Φ_α is the flux of atmospheric neutrinos of type $\alpha = \mu, e$; E_β is the final charged lepton energy and $\varepsilon(E_\beta)$ is the detection efficiency for such charged lepton; σ is the neutrino-nucleon interaction cross section, and θ_ν is the angle between the vertical direction and the incoming neutrinos ($\cos\theta_\nu$=1 corresponds to the down-coming neutrinos). In Eq. (2), h is the slant distance from the production point to the sea level for α-type neutrinos with energy E_ν and zenith angle θ_ν. Finally, κ_α is the slant distance distribution which is normalized to one [17].

The neutrino fluxes, in particular in the sub-GeV range, depend on the solar activity. In order to take this fact into account we use in Eq. (2) a linear combination of atmospheric neutrino fluxes Φ_α^{max} and Φ_α^{min} which correspond to the most active Sun (solar maximum) and quiet Sun (solar minimum), respectively, with different weights, depending on the running period of each experiment [9].

Upgoing muon data are usually presented in the form of measured muon fluxes. We obtain the effective muon fluxes for both stopping and through-going muons by convoluting the probabilities with the corresponding muon fluxes produced by the neutrino interactions with the Earth. We include the muon energy loss during propagation both in the rock and in the detector according to [18,19] and we take into account also the effective detector area for both types of events, stopping and through-going. Schematically

$$\Phi_\mu(\theta)_{S,T} = \frac{1}{A(L,\theta)} \int \frac{d\Phi_\mu(E_\mu,\theta)}{dE_\mu} A_{S,T}(E_\mu,\theta) \quad (3)$$

where

$$\frac{d\Phi_\mu}{dE_\mu} = \int \frac{d\Phi_{\nu_\mu}(E_\nu,\theta)}{dE_\nu} P_{\mu\mu} \frac{d\sigma}{dE_{\mu 0}} R(E_{\mu 0}, E_\mu) \\ \kappa_\mu(h, \cos\theta_\nu, E_\nu) dE_{\mu 0} dE_\nu dh \qquad (4)$$

where $R(E_{\mu 0}, E_\mu)$ is the muon range function which accounts for the muon energy loss during propagation. $A(L,\theta) = A_S(E_\mu,\theta) + A_T(E_\mu,\theta)$ is the projected detector area for internal path-lengths longer than L. A_S and A_T are the corresponding areas for stopping and through-going muon trajectories. For Super-Kamiokande we compute these effective areas using the simple geometrical picture given in Ref. [20].

Following Ref. [9] we explicitly verify in our present reanalysis the agreement of our predictions with the experimental Monte Carlo predictions, leading to a good confidence in the reliability of our results.

3. Conversion Probabilities

For definiteness I assume a two-flavour scenario. For the oscillation case one must solve the Schröedinger evolution equation of the $\nu_\mu - \nu_X$ (where $X = e, \tau$ or s sterile) system in the matter background for *neutrinos*

$$i \frac{\mathrm{d}}{\mathrm{d}t} \begin{pmatrix} \nu_\mu \\ \nu_X \end{pmatrix} = \begin{pmatrix} H_\mu & H_{\mu X} \\ H_{\mu X} & H_X \end{pmatrix} \begin{pmatrix} \nu_\mu \\ \nu_X \end{pmatrix} \ , \quad (5)$$

$$H_\mu = V_\mu + \frac{\Delta m^2}{4E_\nu}\cos 2\theta_{\mu X} \quad (6)$$

$$H_X = V_X - \frac{\Delta m^2}{4E_\nu}\cos 2\theta_{\mu X}, \quad (7)$$

$$H_{\mu X} = -\frac{\Delta m^2}{4E_\nu}\sin 2\theta_{\mu X}, \quad (8)$$

where

$$V_\tau = V_\mu = \frac{\sqrt{2}G_F\rho}{M}(-\frac{1}{2}Y_n)\,, \quad (9)$$

$$V_s = 0\,, \quad (10)$$

$$V_e = \frac{\sqrt{2}G_F\rho}{M}(Y_e - \frac{1}{2}Y_n) \quad (11)$$

Here G_F is the Fermi constant, ρ is the matter density in the Earth, M is the nucleon mass, and Y_e (Y_n) is the electron (neutron) fraction. I define $\Delta m^2 = m_2^2 - m_1^2$ in such a way that if $\Delta m^2 > 0$ ($\Delta m^2 < 0$) the neutrino with largest muon-like component is heavier (lighter) than the one with largest X-like component. For anti-neutrinos the signs of potentials V_X should be reversed. In our calculations we have used the approximate analytic expression for the matter density profile in the Earth obtained in Ref. [21]. In order to obtain the oscillation probabilities $P_{\alpha\beta}$ we have made a numerical integration of the evolution equation. The probabilities for neutrinos and anti-neutrinos are different because the reversal of sign of matter potential. Notice that for the $\nu_\mu \to \nu_\tau$ case there is no matter effect and the probability takes the well known form

$$P_{\mu\mu} = 1 - \sin^2 2\theta \sin^2(\frac{\Delta m^2 L}{2E}). \quad (12)$$

For the $\nu_\mu \to \nu_s$ case there are two possibilities depending on the sign of Δm^2. For $\Delta m^2 > 0$ the matter effects enhance *neutrino* oscillations while depress *anti-neutrino* oscillations, whereas for the other sign ($\Delta m^2 < 0$) the opposite holds. In what follows I will not consider the possibility of oscillation into electron neutrinos as it is known to be ruled out by the negative results of the reactor experiment Chooz [22].

I am also going to consider the possibility of FC-neutrino interactions of massless neutrinos which can also induce $\nu_\mu \to \nu_\tau$ transitions [12]. In our phenomenological approach we have assumed that the evolution equations which describe $\nu_\mu \to \nu_\tau$ transitions in matter may be written as Eq.(5) with

$$H_\mu = 0 \qquad H_\tau = \sqrt{2}\; G_F \epsilon'_\nu n_f(r) \quad (13)$$

$$H_{\mu\tau} = \sqrt{2}\; G_F \epsilon_\nu n_f(r) \quad (14)$$

where $\sqrt{2}\,G_F n_f(r)\epsilon_\nu$ is the $\nu_\mu + f \to \nu_\tau + f$ forward scattering amplitude and $\sqrt{2}\,G_F n_f(r)\epsilon'_\nu$ is the difference between the $\nu_\tau - f$ and $\nu_\mu - f$ elastic forward scattering amplitudes, with $n_f(r)$ being the number density of the fermions which induce such processes. The parameters ϵ_ν and ϵ'_ν contain the information about FC–neutrino interactions, for details I refer to Ref. [12]. In order to obtain the oscillation probabilities $P_{\alpha\beta}$ we have made a numerical integration of the evolution equation. For the sake of illustration I show here the solution in the approximation of constant matter density. The conversion probability in this case is

$$P_{\mu\mu} = 1 - \frac{4\epsilon_\nu^2}{4\epsilon_\nu^2 + {\epsilon'_\nu}^2}\sin^2(\frac{1}{2}\eta L), \quad (15)$$

where $\eta = \sqrt{4\epsilon_\nu^2 + {\epsilon'_\nu}^2}\sqrt{2}G_F n_f$.

Finally when discussing the possibility of neutrino decay in the ν_μ ν_τ system one must include also the effect of the neutrino instability when solving the time evolution of the mass eigenstates. In this case the evolution equation can be solved analytically and the muon neutrino survival probability is given by:

$$P_{\mu\mu} = \sin^4\theta + \cos^4\theta \exp\left(-\frac{m_2}{E}\frac{L}{\tau}\right) + P_{\Delta m^2} \quad (16)$$

with

$$P_{\Delta m^2} = \frac{1}{2}\sin^2 2\theta \cos\left(\frac{\Delta m^2 L}{2E}\right)\exp\left(-\frac{m_2}{E}\frac{L}{2\tau}\right)$$

where τ is the neutrino lifetime. For clarity, I isolated the term $P_{\Delta m^2}$, explicitly dependent on the mass difference, $\Delta m^2 = m_2^2 - m_1^2$. In the following I will neglect this term which averages out in the limit $m_1 \ll m_2 \ll E$. The factor m_2/E in the exponential is just the γ Lorentz factor.

By comparing Eqs.(12), (15), and (16) one can see that the different mechanisms lead to different energy dependence of the survival probability.

While oscillations give a muon survival probability slowly growing with the energy, neutrino decay leads to a much faster growth. On the other hand, flavour changing neutrino interactions lead to an energy independent survival probability. As pointed out in the previous section, data on contained events and upgoing muons scan a range of neutrino energies over three orders of magnitude from hundreds of MeV to hundreds of GeV. This is of great importance when discriminating between the different scenarios as pointed out in Refs.[23,24].

4. Atmospheric Neutrino Data Fits

Here I describe our fitting method to determine the atmospheric neutrino conversion parameters for the various possible conversion channels. In doing so we have relied on the separate use of the event numbers paying attention to the correlations between the errors in the muon predictions and electron predictions as well as the correlations among the errors of the different energy data samples.

The steps required in order to generate the allowed regions of oscillation parameters were given in Ref. [9]. Following Ref. [9,25] we defined the χ^2 as

$$\chi^2 \equiv \sum_{I,J} (N_I^{da} - N_I^{th}) \cdot (\sigma_{da}^2 + \sigma_{th}^2)_{IJ}^{-1} \cdot (N_J^{da} - N_J^{th}), \quad (17)$$

where I and J stand for any combination of the experimental data set and event-type considered, i.e, $I = (A, \alpha)$ and $J = (B, \beta)$ where, A, B stands for the different experiments or different data samples in a given experiment. $\alpha, \beta = e, \mu$. In Eq. (17) N_I^{th} is the predicted number of events calculated from Eq. (1) whereas N_I^{da} is the number of observed events. In Eq. (17) σ_{da}^2 and σ_{th}^2 are the error matrices containing the experimental and theoretical errors respectively. They can be written as

$$\sigma_{IJ}^2 \equiv \sigma_\alpha(A)\, \rho_{\alpha\beta}(A,B)\, \sigma_\beta(B), \quad (18)$$

where $\rho_{\alpha\beta}(A, B)$ stands for the correlation between the α-like events in the A-type experiment and β-like events in B-type experiment, whereas $\sigma_\alpha(A)$ and $\sigma_\beta(B)$ are the errors for the number of α and β-like events in A and B experiments, respectively. The dimension of the error matrix varies depending on the combination of experiments included in the analysis.

We have computed $\rho_{\alpha\beta}(A, B)$ as in Ref. [25]. A detailed discussion of the errors and correlations used in our analysis for the contained events can be found in Ref. [9]. In our present analysis, we have also included the data on stopping and through-going muons. We have conservatively ascribed a 20% uncertainty to the absolute neutrino flux, in order to generously account for the spread of predictions in different neutrino flux calculations. Other important source of theoretical uncertainty arises from the neutrino interaction cross section which at Super-Kamiokande ranges from 10–15 %. We allow a 5% variation in the ratio between muon events in different energy samples. We further introduce a 10% theoretical error in the ratio of electron-type to muon-type events of the different samples. Uncertainties in the ratio between different angular bins are treated, similarly to Ref. [25]. With our definitions we obtain, for instance, χ^2_{SM} =122/(35 d.o.f) which means that the SM has a CL of 10^{-11} !

Next we minimize the χ^2 function in Eq. (17) and determine the allowed region in the parameter space for certain conversion mechanism and for a given confidence level, defined as, $\chi^2 \equiv \chi^2_{min} + 4.61$ (9.21) for 90 (99) % C.L.

In Table 1 I show the minimum value of χ^2 and the best fit point for several conversion mechanisms and for the different data sets.

The results of our χ^2 fit of the Super-Kamiokande contained and upgoing atmospheric neutrino data in the framework of neutrino oscillations are given in Fig. (1). In this figure I give the allowed region of oscillation parameters at 90 and 99 % CL.

One can notice that matter effects lead to differences between the allowed regions in the different channels. In the case of $\nu_\mu \to \nu_s$ with $\Delta m^2 > 0$ matter effects enhance the oscillations for *neutrinos* and therefore smaller values of the vacuum mixing angle would lead to larger conversion probabilities and the regions are therefore larger as compared to the vacuum case $\nu_\mu \to \nu_\tau$. In the case of $\nu_\mu \to \nu_s$ with $\Delta m^2 < 0$ the enhance-

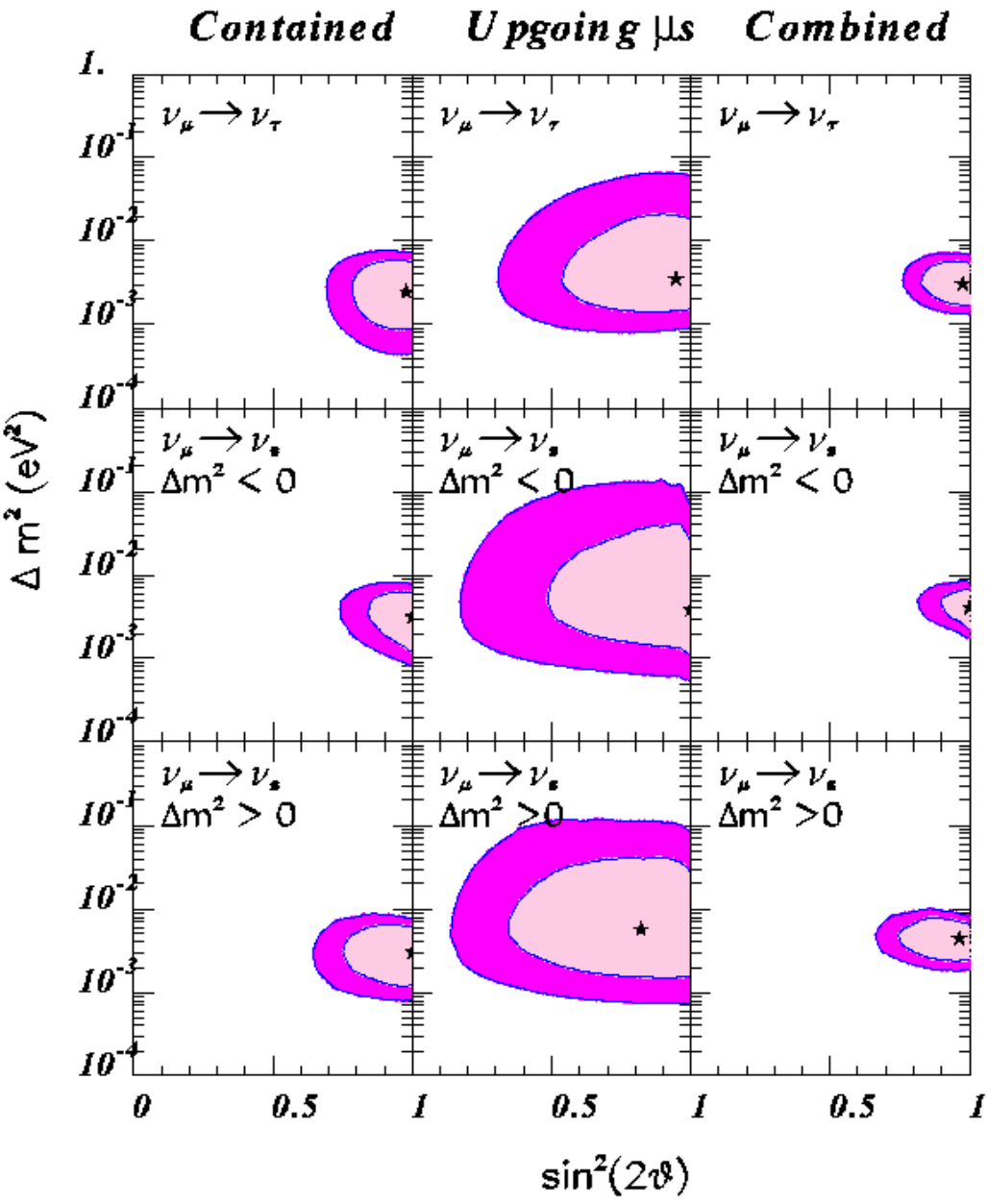

Figure 1. Allowed regions of the oscillation parameters for the different Super-Kamiokande data samples and oscillation channels as labelled in the figure.

ment occurs only for *anti-neutrinos* while in this case the effect of matter suppresses the conversion in ν_μ's. Since the yield of atmospheric neutrinos is bigger than that of anti-neutrinos, clearly the matter effect suppresses the overall conversion probability. Therefore one needs in this case a larger value of the vacuum mixing angle, as can be seen by comparing the regions in the second row with the corresponding ones in the first and third row in Fig. (1).

Notice that in all channels where matter effects play a role the range of acceptable Δm^2 is slightly shifted towards larger values, when compared with the $\nu_\mu \to \nu_\tau$ case. This follows from looking at the relation between mixing *in vacuo* and in matter. In fact, away from the resonance region, independently of the sign of the matter potential, there is a suppression of the mixing inside the Earth. As a result, there is a lower cut in the allowed Δm^2 value, and it lies higher than what is obtained in the data fit for the $\nu_\mu \to \nu_\tau$ channel.

Concerning the quality of the fits we see in table 1 that the best fit to the full sample is obtained for the $\nu_\mu \to \nu_\tau$ channel although from the global analysis oscillations into sterile neutrinos cannot be ruled out. One can also observe an improvement in the quality of the fits to the contained events as compared to previous analysis performed with lower statistics [9]. These features can be easily understood by looking at the predicted zenith angle distribution of the different event type for the various oscillation channels which I show in Fig. (2) for contained events and Fig. (3) for upgoing muons. In Fig. (2) we observe a perfect agreement between the observed distributions of e-like events and the predictions in the SM. This has lead to an improvement of the quality of the description for any conversion mechanism that only involves muons. Also in Fig. (3) we can observe that due to matter effects the distribution for upgoing muons in the case of $\nu_\mu \to \nu_s$ are flatter than for $\nu_\mu \to \nu_\tau$ [23,20]. Data show a somehow steeper angular dependence which can be better described by $\nu_\mu \to \nu_\tau$. This leads to the better quality of the global fit in this channel. Pushing further this feature Super-Kamiokande collaboration has presented a preliminary partial analysis of the angular dependence of the through-going muon data in combination with the up-down asymmetry of partially contained events which seems to exclude the possibility $\nu_\mu \to \nu_s$ at the 2–σ level [2].

5. Alternative Scenarios

As we have seen in the previous section the oscillation hypothesis provides a very good explanation to the atmospheric neutrino data, and it is also simple and well-motivated theoretically. However, alternative explanations to the atmospheric neutrino data have been proposed in the literature. In this section I concentrate on the present status of two possible "exotic"scenarios: FC-neutrino interactions in the Earth matter [12] and neutrino decay [13].

In Fig. (4) I show the allowed regions in the parameter space for the decay mechanism $\nu_\mu \to \nu_\tau X$ for Super-Kamiokande sub-GeV and multi-GeV events separately as well as the combined contained events. Partial fits to the two events samples lead to rather good description as can be seen in Table 2. However the description of the global contained event sample is considerably worse than in the case of oscillations. This arises from the stronger energy dependence of the survival probability while the contained data both

Table 2
Minimum value of χ^2 and the best fit point to contained events for the decay $\nu_\mu \to \nu_\tau X$.

Experiment		
Super-Kam sub-GeV	χ^2_{min}	1.4
	m/τ (10^{-5} GeV/Km)	8.1
	$\sin^2\theta$	0.05
Super-Kam multi-GeV	χ^2_{min}	5.9
	m/τ (10^{-5} GeV/Km)	31.
	$\sin^2\theta$	0.1
Super-Kam Contained	χ^2_{min}	21.9
	m/τ (10^{-5} GeV/Km)	9.3
	$\sin^2\theta$	0.07

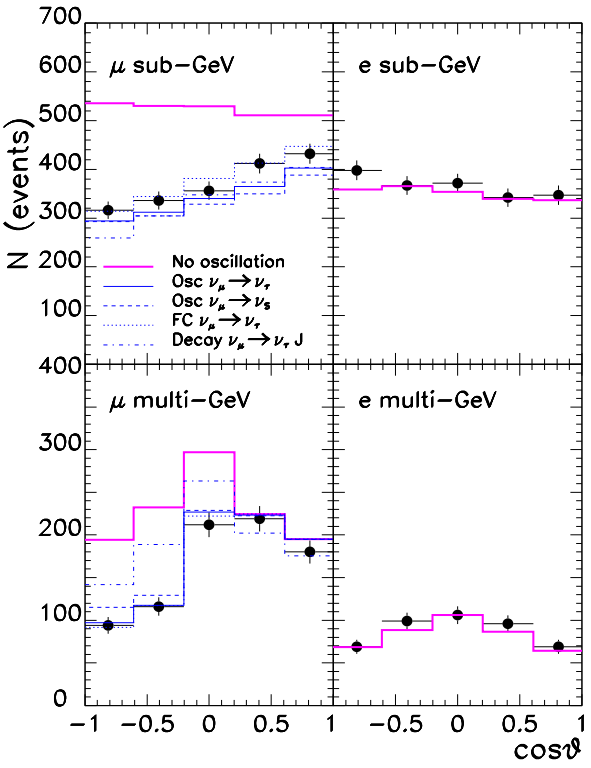

Figure 2. Angular distribution for Super-Kamiokande electron-like and muon- like sub-GeV and multi-GeV events together with our prediction in the absence of oscillation as well as the prediction for the best fit point to the contained event data for the different conversion mechanism as labelled in the figure. The error displayed in the experimental points is only statistical.

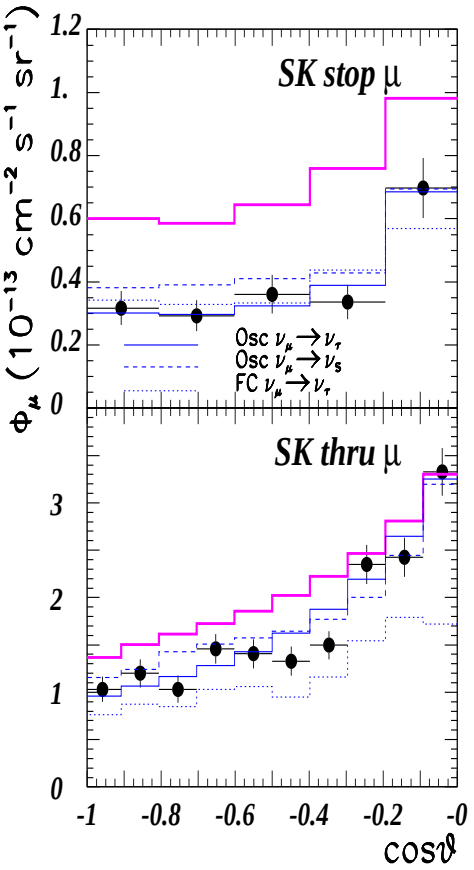

Figure 3. Angular distribution for Super-Kamiokande upgoing muon data together with our prediction in the absence of oscillation as well as the prediction for the best fit point to the full data sample for the different conversion mechanism as labelled in the figure.

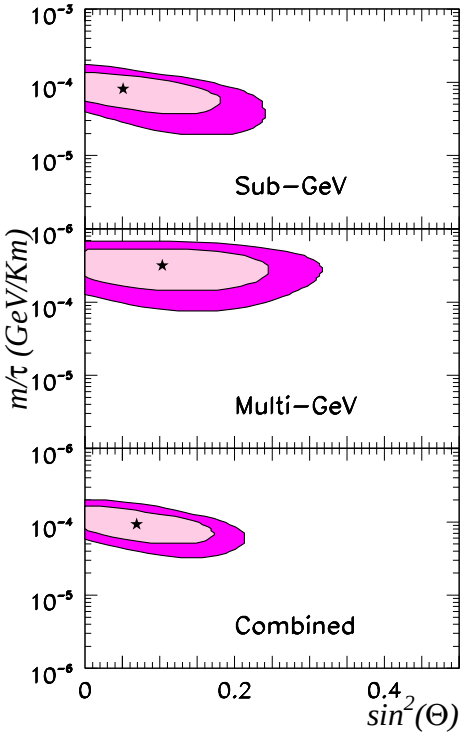

Figure 4. Allowed regions of th neutrino decay parameters for the different Super-Kamiokande data samples.

in the sub-GeV and multi-GeV samples present a similar deficit. As a consequence the allowed decay lifetimes which give a good description to the sub-GeV and multi-GeV data present very little overlap as can be observed by comparing the upper and central panels in Fig. (4). As a consequence the mechanism gives a worse fit to the global contained sample. This can also be observed in the angular distribution of contained events for the best fit to the contained events (dash-dotted line in Fig. (2)) from where one sees that the decay hypothesis cannot produce enough up-down asymmetry for the multi-GeV sample without conflicting with the sub-GeV data.

This behaviour becomes particularly lethal when trying to describe the upward going muon data since for lifetimes favoured by the contained event data very little muon conversion is expected already for stopping muons in contradiction with observation. Based on this fact this mechanism was ruled out in its simpler form in Ref. [23,24] Recently the possibility of neutrino decay in a more general four neutrino scenario has been revisited in Ref.[26] where it is discussed that a good description to the full atmospheric data sample is possible.

I finally discuss our results on the alternative explanation of the atmospheric neutrino data in terms of FC neutrino-matter interactions [12]. In Fig. (5) I show the contours of the regions allowed by the Super-Kamiokande data. The different panels of the figure refer to the fits performed over the different sets of data. The shaded areas are the regions allowed at 90% C.L., while the dashed and dotted contours refer to 95 and 99 % C.L., respectively. In Table 1 I list the corresponding best fit points as well as the values of χ^2_{min} attainable for this mechanism. From the table we see that contained and stopping muon events can be described with a quality comparable to the oscillation channels. In Fig.(2) one can also observed that the FC-neutrino mechanism leads to a very good description of the zenith angular distributions for contained events. This may come as a surprise since angular distributions for multi-GeV and sub-GeV events are rather different while the FC mechanism leads to an energy independent conversion probability. One must bear in mind,

however, that the plotted angular distribution is that of the produced charged leptons in the neutrino interaction. For neutrinos leading to sub-GeV events the average opening angle between the neutrino and the produced lepton is 60 degrees what leads to the flat observed distribution almost independently of the specific conversion mechanism. The overall normalization, is however, totally consistent with the FC hypothesis as the deficit in both samples is of about 60 %.

The allowed regions can be qualitatively understood in the approximation of constant matter density in Eq.(15). From there one can see that in order to have a relatively large transition probability, as implied by the contained events and also by the stopping muons events, the FC parameters are required to be in the region $\epsilon'_\nu < \epsilon_\nu$ and $\eta > \pi/R_\oplus$. This last condition leads to a lower bound on ϵ_ν. The island in Fig. (5.a) corresponds to $\eta \sim \pi/R_\oplus$. On the other hand, the through-going muon data require a smaller transition probability and therefore the region $\epsilon'_\nu > \epsilon_\nu$ turns out to be the preferred one.

The combination of the different data sets in a single χ^2-analysis is shown in Fig. (5.d). As seen in the figure as well as in Table 1, when the angular information of both stopping and through-going muons is included in the data analysis, the quality of the full description worsens and leads to a $\chi^2_{min} = 43.8/(33 d.o.f)$. Since FC-neutrino interactions lead to an energy independent conversion probability, the smaller deficit in the through-going muon sample as compared to contained and stopping-muon samples cannot be well accommodated. As seen in the lower panel in Fig. (3) the prediction for the best fit point for this mechanism would imply a larger deficit for higher energy muons mainly in the last three angular bins where it does not produce a sufficient amount of through-going muons at angles $0 < \theta < 20$ degrees below the horizon.

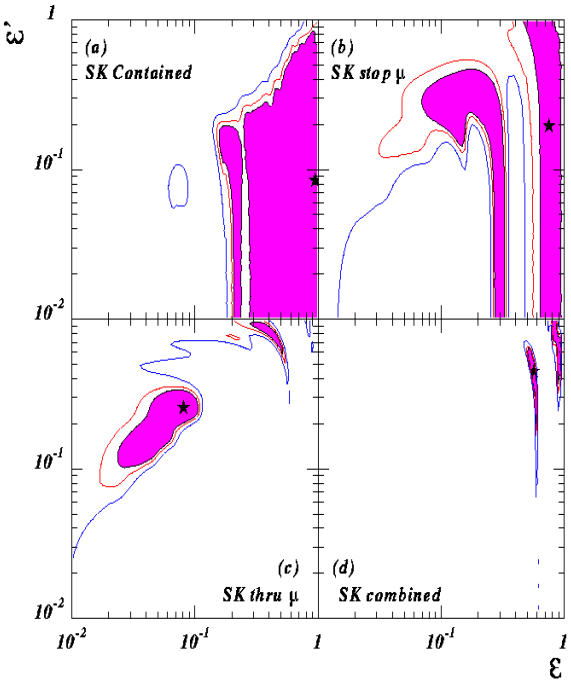

Figure 5. Allowed regions of the FC-neutrino interactions parameters for the different Super-Kamiokande data samples.

REFERENCES

1. Y. Fukuda *et al.*, Phys. Lett. **B433**, 9 (1998); Phys. Lett. **B436**, 33 (1998);
2. M. Nakahata, talk at *Sixth International Workshop on Topics in Astroparticle and Un-*

derground Physics, TAUP99, Paris September 1999.
3. K. Daum *et al.* Z. Phys. **C66**, 417 (1995).
4. M. Aglietta *et al.*, Europhys. Lett. **8**, 611 (1989).
5. H. S. Hirata *et al.*, Phys. Lett. **B280**, 146 (1992); Y. Fukuda *et al.*, *ibid* **B335**, 237 (1994).
6. R. Becker-Szendy *et al.*, Phys. Rev. **D46**, 3720 (1992).
7. W. W. M. Allison *et al.*, Phys. Lett. **B449**, 137 (1999).
8. G. Barr, T. K. Gaisser and T. Stanev, Phys. Rev. **D 39** (1989) 3532 and Phys. Rev. **D38**, 85; V. Agrawal *et al.*, Phys. Rev. **D53**, 1314 (1996); M. Honda, T. Kajita, S. Midorikawa and K. Kasahara, Phys. Rev. **D52**, 4985 (1995).
9. M. C. Gonzalez-Garcia, H. Nunokawa, O. L. G. Peres, T. Stanev and J. W. F. Valle, Phys. Rev. **D58**, 033004 (1998); M.C. Gonzalez-Garcia, H. Nunokawa, O.L. Peres and J. W. F. Valle, Nucl. Phys. **B543**, 3 (1999), hep-ph/9807305.
10. R. Foot, R. R. Volkas and O. Yasuda, Phys. Rev. **D58**, 013006 (1998); O. Yasuda, Phys. Rev. **D58**, 091301 (1998); G. L. Fogli, E. Lisi, A. Marrone, G. Scioscia, Phys. Rev. **D59**, 033001 (1999) ep-ph/9808205; E.Kh. Akhmedov, A.Dighe, P. Lipari and A.Yu. Smirnov, hep-ph/9808270.
11. Y. Fukuda *et al.*, Phys. Rev. Lett. **81**, 1562 (1998).
12. M.C. Gonzalez-Garcia, M.M. Guzzo, P.I. Krastev, H. Nunokawa, O.L.G. Peres, V. Pleitez, J.W.F. Valle and R. Zukanovich Funchal, Phys. Rev. Lett. **82**, 3202 (1999); N. Fornengo, M.C. Gonzalez-Garcia, J.W.F. Valle hep-ph/9906539.
13. V. Barger, J.G. Learned, S. Pakvasa, and T.J. Weiler, Phys. Rev. Lett. **82**, 2640 (1999).
14. M. Gasperini, Phys. Rev. **D38**, 2635 (1988); J. Pantaleone, A. Halprin, C.N. Leung, Phys. Rev. **D47**, 4199 (1993); A. Halprin, C.N. Leung, J. Pantaleone Phys. Rev. **D53**, 5365 (1996).
15. S. Coleman, S. L. Glashow, Phys. Lett. **B405**, 249 (1997); S. L. Glashow, A. Halprin, P.I. Krastev , C.N. Leung, J. Pantaleone, Phys. Rev. **D56**, 2433 (1997).
16. S. Coleman, S. L. Glashow, Phys. Rev. **D59**, 116008 (1999).
17. T. K. Gaisser and T. Stanev, Phys. Rev. **D57** 1977 (1998).
18. W. Lohmann, R. Kopp and R. Voss, CERN Yellow Report EP/85-03.
19. E. Zas, F. Halzen, R.A. Vazquez, Astropart. Phys. **1** 297 (1993).
20. P. Lipari, M. Lusignoli Phys. Rev. **D58**, 073005 (1998).
21. E. Lisi and D. Montanino, Phys. Rev. **D56**, 1792 (1997).
22. CHOOZ Collaboration, M. Apollonio *et al.*, Phys. Lett. B **420** 397(1998).
23. P. Lipari, M. Lusignoli Phys. Rev. **D60**, 013003 (1999).
24. G.L. Fogli, E. Lisi, A. Marrone, G. Scioscia, Phys. Rev. **D59**, 117303 (1999); *ibid* **D60**, 053006 (1999).
25. G. L. Fogli, E. Lisi, Phys. Rev. **D52**, 2775 (1995); G. L. Fogli, E. Lisi and D. Montanino, Phys. Rev. **D49**, 3626 (1994); Astrop. Phys. **4**, 177 (1995); G. L. Fogli, E. Lisi, D. Montanino and G. Scioscia Phys. Rev. **D55**, 485 (1997).
26. V. Barger, J.G. Learned, P. Lipari, M. Lusignoli,S. Pakvasa, and T.J. Weiler, hep-ph/9907421.

Table 1
Minimum value of χ^2 and the best fit point for each channel and for different data sets.

Experiment	Oscillation	$\nu_\mu \to \nu_\tau$	$\nu_\mu \to \nu_s$ $\Delta m^2 < 0$	$\nu_\mu \to \nu_s$ $\Delta m^2 > 0$	FC ν-matter
Super-Kam	χ^2_{min}	8.8	12.9	12.6	9.4
contained	Δm^2 (10^{-3}eV^2)	2.5	3.2	3.0	ϵ=0.95
d.o.f=20-2	$\sin^2 2\theta$	0.98	1.	0.99	ϵ'=0.084
Super-Kam	χ^2_{min}	1.3	2.4	2.3	1
Stopping–μ	Δm^2 (10^{-3}eV^2)	3.0	3.3	3.7	ϵ=0.76
d.o.f=5-2	$\sin^2 2\theta$	0.99	1.	0.93	ϵ'=0.19
Super-Kam	χ^2_{min}	10.4	13.4	10.5	10.4
Through-Going–μ	Δm^2 (10^{-3}eV^2)	10.0	4.9	18.	ϵ=0.08
d.o.f=10-2	$\sin^2 2\theta$	0.78	1.	0.55	ϵ'=0.26
Super-Kam	χ^2_{min}	23.5	32.9	32.5	43.8
Combined	Δm^2 (10^{-3}eV^2)	3.1	4.1	4.5	ϵ =0.57
d.o.f=35-2	$\sin^2 2\theta$	0.98	1.	0.96	ϵ'=0.45